Design, Characterization and Optimization of a Soft Fluidic Actuator for Minimally Invasive Surgery

Gilles Decroly[1] · **Benjamin Mertens**[1] ·
Pierre Lambert[2] · **Alain Delchambre**[1]

Abstract Purpose In minimally invasive surgery and endoscopy, the rise of soft robotics, using materials of similar softness as biological soft tissues, opens many new opportunities. Soft actuated catheters could become an alternative to current steerable catheters, by minimizing the risk of damage to surrounding tissues while enhancing the possibilities to navigate in confined space and to reach remote locations. Fluidic actuators present the advantage to be safe, since they do not require rigid parts nor voltage, to be lightweight, and to allow the reduction of the number of parts needed for a given movement. This work presents the design, development and characterization of a soft fluidic bending actuator for a steerable catheter. **Methods** A silicone prototype of 5 mm diameter has been designed. It has one degree of freedom in bending and achieves a radius of curvature below 10 mm. A numerical model has been developed and compared to the experimental results. **Results** Despite an overestimation of the bending, the numerical model properly captures the behaviour of the actuator. This allowed to identify and validate the key design parameters of the actuator, namely the ratio between the pressure channel surface and the actuator cross-section surface. Based on the results, an optimized design has been developed and numerically implemented. The miniaturization and the potential to carry devices with non-negligible bending stiffness have also been discussed. **Conclusion** In this work, a proof of concept of a soft fluidic actuator for a steerable catheter has been designed, developed and characterized. It showed promising results concerning the feasibility of a miniaturized actuator with two degrees of freedom.

Keywords Soft robotics · Fluidic actuator · Steerable catheter · Minimally invasive surgery · Finite element modelling

Gilles Decroly
E-mail: gilles.decroly@ulb.ac.be

1

Université libre de Bruxelles, BEAMS Department
50 Av. Franklin Roosevelt, 1050 Brussels, Belgium

2

Université libre de Bruxelles, TIPs Department
50 Av. Franklin Roosevelt, 1050 Brussels, Belgium

1 Introduction

Soft robotics is an emerging field presenting various applications such as grippers, wearable devices or minimally invasive surgery (MIS) tools [1–3]. MIS requires specific devices, such as endoscopes and catheters. Several solutions have been suggested to actuate steerable navigation tools [4–6]. They can be sorted into four main actuation methods: cable actuation, magnetic actuation, smart material actuation, and fluidic actuation. The emergence of soft robotics, associated with fluidic and smart materials actuation, is bringing new possibilities, as well as enabling a new paradigm for navigation tools, in terms of softness and safety, to achieve more complex movements and to develop inexpensive actuators [2]. Such tools could enable reaching locations through tortuous trajectories in the human body while minimizing the risk of damaging tissues and presenting low interaction force with organs [1, 3, 7]. Several reviews on the actuation methods for soft robotics can be found in the literature [1, 2, 8, 9]. Among those solutions, fluidic actuation seems especially promising for MIS applications. The bending is achieved using the deformation generated by fluidic pressure on the walls of a chamber, combined with anisotropic rigidity. This solution has the benefit of being safe, since it does not require parts under voltage [9], of being made entirely of compliant material [1], as well as being lightweight [1, 9]. Also, the fluidic actuation allows the reduction of the number of parts needed for a given movement [9].

Since the design suggested by Suzumori [10], many designs have been proposed in the literature with diameters as low as 1.7 mm, but containing no or too small internal lumen and having non-constant cross-sections [11, 12]. A constant cross-section geometry offers the advantage of being easily produced. These designs have generally external diameter wider than 10 mm or no internal lumen [13–17]. At large scale, a colonoscope using this solution has already been commercialized (Endotics, ERA endoscopy). Sun [18] proposed a very promising design, based on a combination of eccentric and multi-material asymmetry with an internal lumen and an external diameter of 6 mm. Recently, research focused on the integration of such soft robots in robotic platforms, and its benefits for specific procedures have been demonstrated, for example, to provide a better field of vision during laparoscopic procedures in the low pelvis [19].

This work presents the design, characterization and optimization of a miniaturized soft fluidic actuator for steerable catheter, able to develop radius of curvature smaller than 10 mm. The novelty of this multi-purpose design is to integrate an internal lumen, which allows carrying a MIS device (i.e. the leads of a camera) while being miniaturized to 5 mm outer diameter. This actuator could be used as an end effector on a steerable catheter, to reach locations inaccessible to endoscopes and laparoscope and increase the surgeon's dexterity. The miniaturized actuator is introduced in subsection 2.1 and the manufacturing is described in subsection 2.2. A numerical model is developed in subsection 2.3, and the experimental method is given in subsection 2.4. The results are compared in section 3. The models are first validated based on the experimental results, allowing to identify the key design parameters of the actuator in a second phase. Based on the results, an optimization study is presented using the numerical model. A design able to bend in every direction is proposed, to enhance navigation capabilities. The potential applications and use cases are discussed in subsection 3.4, studying the effect of the tool placed
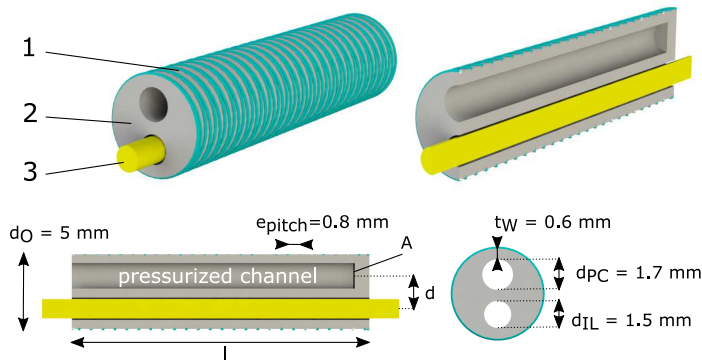
Fig. 1 Implemented actuator design. (1) Fibre reinforcement. (2) Soft silicone body. (3) Limiting fibre/leads of the MIS device.

in the internal lumen and the potential for further miniaturization. Propositions for future work directions conclude the paper.

2 Materials and Methods

2.1 Design

The implemented design is presented in Figure 1. It has one degree of freedom in bending and an outer diameter $d_{\mathrm{O}} = 5\,\mathrm{mm}$. Three main parts are composing the actuator: a soft silicone body, a fibre reinforcement, and a strain limiting fibre. The soft body is made of silicone and integrates two channels: a pressurized channel (diameter $d_{\mathrm{PC}} = 1.7\,\mathrm{mm}$) and a internal lumen (diameter $d_{\mathrm{IL}} = 1.5\,\mathrm{mm}$). The wall thickness is consequently $t_{\mathrm{W}} = 0.6\,\mathrm{mm}$. One of the advantages of the design is the constant cross-section of the actuator, significantly simplifying the design and assembly. Fibre reinforcement is added externally, to limit the radial expansion of the soft body, and does not increase the bending stiffness of the actuator. This fibre reinforcement is mainly characterized by its pitch, i.e. the distance between two turns, which is set at $e_{\mathrm{pitch}} = 0.8\,\mathrm{mm}$. Wang [20] studied the influence of the pitch on the bending and showed that from a critical value, the bending angle is maximal and the pitch does not influence the bending. This critical value of pitch is reached when the radial expansion is utterly constrained, i.e. when no "bubble" appears between the fibres. The limiting fibre plays an essential double role in the bending. It acts as neutral fibre, limiting the elongation of the actuator, and inducing the bending. Also, the leads of the MIS device placed in the internal lumen (typically a camera) can directly act as strain limiting fibre, here implemented by a thread.

Euler-Bernoulli beam theory can be used to provide a first interpretation of the working principle of the actuator. The pressure is evenly distributed on the pressurized channel surface. The radially directed pressure will only induce a radial deformation of the actuator, assumed entirely prevented here by the fibre reinforcement. The pressure p applied on the area A of the tip of the pressurized channel will result in an axial force F shifted of a distance d relatively to the neutral fibre, whose position is imposed by the limiting fibre. The generated moment

$M = p.d.A$, constant along the length of the actuator, causes the bending of the actuator with an angle θ. The radius of curvature $R_C = l/\theta$, independent of the length l is then used to characterize the bending. The bending is inversely proportional to the bending stiffness of the actuator, which depends on the material and geometrical properties of the material, especially the diameter of the actuator.

The designs presented in this section will be further studied in subsection 2.3 and subsection 2.4. Based on the results, an optimisation of the design is proposed in subsection 3.3.

2.2 Manufacturing

The soft body is made of moulded silicone (Ecoflex 0030, Smooth-On). The moulding process is inspired by the Inverse Flow Injection process described by Sun [18]. This process allows the production of soft bodies of sufficient quality, i.e. with clean and constant cross-sections, and repeatable. Silicone glue is used to seal the pressurized channel and to fix the pressure connection tube and the limiting fibre. Two helix winding (left- and right-handed) of fibre reinforcement are added manually. A 0.15 mm diameter polyester suture thread is used as fibre. A thin layer of silicone is added after the placement of the thread to fix it. The limiting fibre is implemented with a polyester suture thread of 0.6 mm diameter.

2.3 Modelling

A quasi-static numerical finite element model has been developed on COMSOL Multiphysics. The geometry of the numerical model is shown in Figure 3. The parameters are based on the value of the designed geometry, excepted for the length, which differs between the different samples; the thickness of the sealing of the pressurized channel, which had to be estimated; and the limiting fibre diameter. The dynamics of the actuator is not considered here, the surgeon movements being comprised below 2 Hz during normal procedure [15], and the typical order of magnitude for fluidic actuator bandwidth being around 10 Hz [2]. Several simplifications are assumed. Seeing its role (subsection 2.1), the double helix is modelled by an array of a torus. This assumption allows a drastic simplification of the geometrical model. The reinforcement fibre is modelled squared and placed externally to the actuator, the additional fixation silicone layer is not considered. To avoid contact boundary conditions, the limiting fibre is placed in the silicone. The diameter of this limiting fibre has been reduced by a factor of two [21], to limit the bending stiffness of the fibre while maintaining its length limiting properties. The symmetrical properties of the actuator have been used to reduce the computational cost, and the weight is not taken into consideration. A fixed boundary constraint is applied on the proximal surface of the silicone body, and a pressure load is applied on the pressure channel surface. A third order incompressible Yeoh model is used to model the hyperelastic silicone body. It describes the material by its strain energy density W_s as a function of the strain invariants I_1 [22]: $W_s = c_1(I_1 - 3) + c_2(I_1 - 3)^2 + c_3(I_1 - 3)^3$. Kulkarni's characterization of Ecoflex 0030 [23] is implemented, with coefficients $c_1 = 12.7\,\mathrm{kPa}$, $c_2 = 423\,\mathrm{Pa}$, and $c_3 = -1.46\,\mathrm{Pa}$. The incompressibility is implemented by using a
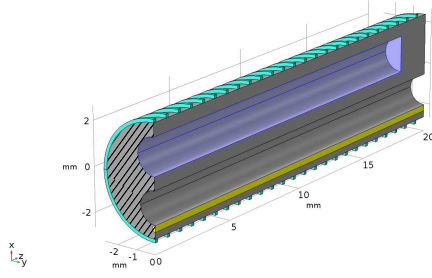
Fig. 2 Geometry of the numerical model for the angle measurement. The hatched surface indicates a fixed boundary condition. A pressure load is applied on the surface of the pressurized channel (in light blue).

high initial bulk modulus (100 MPa). The density is $1.07\,\text{g/cm}^3$. As proposed by Polygerinos [21], the fibre reinforcement is modelled by a linear elastic material, having a Young's modulus of $E = 31.076\,\text{MPa}$ and a Poisson's ratio of $\nu = 0.36$. The inextensible limiting fibre is modelled by an incompressible Yeoh model with $c_1 = 7.9\,\text{MPa}, c_2 = 0, c_3 = 0$ [21]. Default second order tetrahedral elements are used for the meshing of the actuator. Boundary layers are added on the surface subject to the pressure to refine the mesh. A MUMPS direct solver is used, and an auxiliary sweep on the pressure is performed to improve its convergence. The convergence of the model has been validated using the maximal displacement. The simulation takes around 15 min to run. A similar model has been developed to characterize the blocking force developed by the actuator. A fixed surface is placed below and tangent to the actuator, and a contact boundary condition is added between both parts.

The main assumptions of the numerical model have been validated through a sensitivity study, evaluating the influence of the variation of one parameter at a time in a reasonable order of magnitude with respect to possible errors on the fabrication process of the prototypes (Table 1). The parameters related to the fibre reinforcement have a relatively small influence on the radius of curvature. This means that in the range of variation of pitch, thread diameter, and thread shape studied, the radial expansion remains fully constrained, and the bending stiffness of the thread remains negligible [20]. The diameter of the limiting fibre is also a negligible parameter, indicating that the bending stiffness of this fibre remains negligible. Contrarily to the first interpretation, the placement of the limiting fibre, and consequently the distance between the centroid of the pressure channel and the neutral fibre, is not a crucial parameter. The "top" and "bottom" configurations indicate that the fibre is placed in the silicone, respectively above and below the internal lumen. The model without limiting fibre demonstrates its role to optimize the bending. Note that the placement of the limiting fibre in the silicone (and not in the centre of the internal lumen) increases slightly the bending of the model. It is less realistic but makes contact boundary conditions unnecessary and reduces the computational cost of the model. Finally, the material model is of substantial influence, and the different Yeoh hyperelastic material models presented in the literature differ significantly from each other [21]. For further

Table 1 Influence of the assumptions on the numerical model. The radius of curvature is given for a pressure of 0.20 bar (* at 0.15 bar for the placement of the limiting fibre). The lines in bold indicate the value of the parameter used in the implemented model.

Modified parameter	Value	Radius of curvature (mm)
Pitch of the fibre reinforcement	0,50 mm	17,18
	0,80 mm	**16,86**
	1,10 mm	16,31
Reinforcement thread diameter	0.10 mm	16.31
	0.15 mm	**16.86**
	0.20 mm	17.31
Reinforcement thread shape	round	18.04
	rectangular	**16.86**
Limiting fibre diameter	0.2 mm	17.14
	0.3 mm	**16.86**
	0.4 mm	17.01
Limiting fibre placement*	top	31.20
	bottom	**31.13**
	center	33.46
	no fibre	36.36
Hyperelastic material model	Polygerinos [21]	15.01
	Kulkarni [23]	**16.86**

work, the hyperelastic material should be characterized internally, to ensure an adequate model.

2.4 Experimental method

Two tests benches have been developed to characterize the bending using the radius of curvature R_C and the blocking force F of the actuator as a function of the pressure. Their conceptual design is shown on Figure 3. The bending characteristics were measured on six actuators with lengths varying between 16 mm and 48 mm. The blocking force test bench is based on the angle measurement, but the angular graph paper is replaced by a precision weighing scale, used as a force sensor. The weighing scale is placed horizontally to measure the blocking force. Two actuators of $l = 17$ mm long were each tested three times. The initial weight (i.e. the measure for $p = 0$ bar) is subtracted to the measured weight, to isolate the force of the actuator. The tests benches allowed a reproducible characterization of the actuators, despite several limitations. Placing the actuator horizontally adds friction between the actuator and the angular graph paper, and leads to an underestimation of the bending/force if the bending does not happen perfectly in the horizontal/vertical plane.

3 Results and discussion

3.1 Characterization and validation of the numerical model

The radius of curvature of the actuator reaches values smaller than $R_C = 10$ mm for pressures around $p = 0.35$ bar. The numerical model shows similar results in
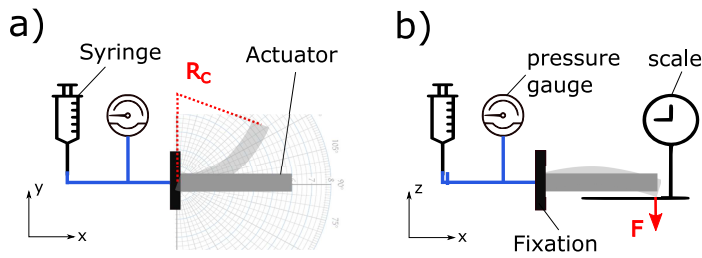
Fig. 3 Conceptual scheme of the test benches. (a) Angle measurement. (b) Blocking force measurement.
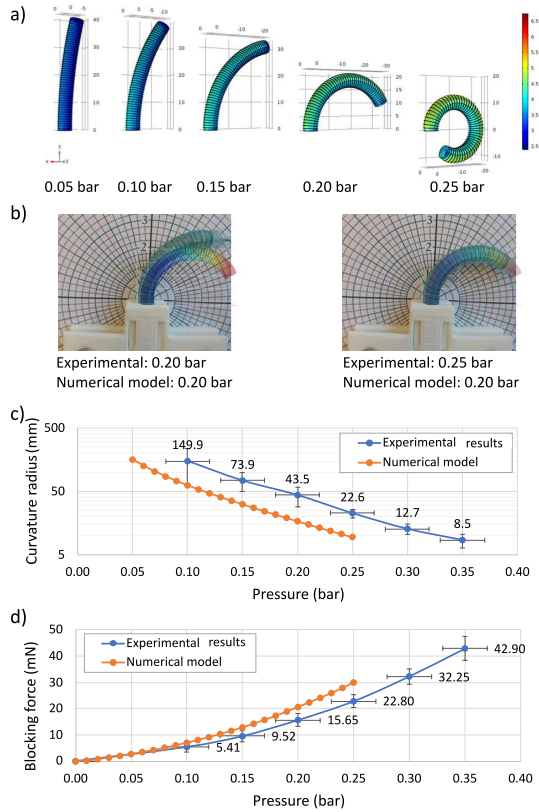
Fig. 4 Results. a) Bending of the numerical model ($l = 40\,\text{mm}$). The colour scale represents the logarithme of the von Mises stress (Pa). b) Superposition of the numerical model ($p = 0.20\,\text{bar}$, $l = 40\,\text{mm}$) and the experimental results (sample C, $p = 0.20\,\text{bar}$ and $p = 0.25\,\text{bar}$, $l = 39\,\text{mm}$). c) and d) Comparison of the results as a function of the pressure. The mean of the experimental results is plotted. The error bars indicate the standard deviation of the measures for the radius of curvature, and the measurement error on the pressure gauge ($\pm 0.02\,\text{bar}$). Radius of curvature: $l = 20\,\text{mm}$; Blocking force: $l = 17\,\text{mm}$.

terms of achievable bending, as illustrated in Figure 4. We can observe that the numerical model is overestimating the bending at a given pressure. However, it superposes almost perfectly with a shift in the input pressure of 25%. This is confirmed by the quantitative comparison using the radius of curvature. The numerical model follows the experimental results despite a shift between the two curves. The numerical and experimental blocking force results allow to characterize the order of magnitude of the blocking force developed by the actuator: around 40 mN for a pressure $p = 0.35$ bar. As for the bending, the numerical model overestimates the blocking force compared to the experimental results. For a given blocking force, the shift of pressure between the experimental results and numerical model is similar to that of the bending model at a given radius of curvature. Note that, as taken into account in the models, no significant hysteresis is observed in the experimental results, where the pressure is increased from 0 bar to 0.35 bar, and then decreased again to 0 bar.

The differences between the experimental results and the numerical models could be explained by the limitations of the experimental setup, the inaccuracies caused by manufacturing, and by the assumptions made on the numerical model. In particular, the friction and the placement imprecision of the actuator on the test bench lead to an underestimation of the bending. Also, the outer diameter of the prototypes is probably decreased by the tension of the thread during the reinforcement, while the external wall thickness is increased by the additional layer of silicone fixing the reinforcement fibres. Finally, the hyperelastic material model used for this study is a limitation. Large variations are found in the literature. The model used in this study only characterized the material under uniaxial loading, while multiaxial deformation happens during inflation of the actuator, which can decrease the model quality [24]. Despite these differences, the numerical models properly capture the behaviour of the actuator. More, the soft actuator achieves a radius of curvature smaller than 10 mm, validating the proof of concept developed in this work.

3.2 Key design parameters

Different geometrical parameters were varied one at a time to identify the key design parameters. Among others, the impact of a small shifting of the pressure channel upwards in the cross-section (decreasing the wall thickness between the pressure channel and the fibre reinforcement) or downwards (decreasing the wall thickness between the internal lumen and the pressure channel) has been studied. The bending is strongly increased when the pressure channel is placed more eccentrically (radius of curvature of 14.19 mm at 0.15 bar with an upwards shift of 0.2 mm, to be compared to the 16.86 mm radius of curvature with no shift, and 18.90 mm radius of radius with a downwards shift of 0.2 mm). Since the distance d between the centroid of the pressurized channel showed only a limited influence (subsection 2.3), this could be explained by the fact that the thinner wall between the channel and the reinforcement fibre requires less pressure to be extended. Note that this decreased thickness goes along with an increased wall fragility. The influence of the other geometrical parameters is synthesized in Figure 5. For each varied parameter, all the other parameters excepted the pressure channel diameter are fixed, allowing only this last parameter to vary. It can be observed that
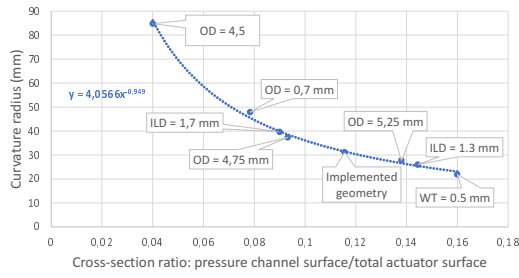
Fig. 5 Simulation results. Radius of curvature as a function or the ratio pressure channel surface/total surface at 0.15 bar (OD: Outer Diameter, WT: Wall Thickness, ILD: Internal Lumen Diameter).

the influence of these parameters can be summarized using the ratio between the surface of the cross-section of the pressure channel and the surface of the cross section of the actuator. This is therefore considered to be the main geometrical parameter, to be maximized to optimize the bending. Those results are coherent with the framework developed analytically by Garriga-Casanovas [25] applied to the present design. Based on these results, optimized designs are presented in subsection 3.3. The potential for further miniaturization and to carry an endoscopic device are studied in subsubsection 3.4.2 and subsubsection 3.4.1.

3.3 Optimized design

Two optimized designs are proposed. They are shown in Figure 6 and present a maximized pressure channel surface. The design with one degree of bending in freedom (1-dof design) should increase the bending and blocking force developed by the actuator for a given pressure. However, to increase the surgeon's dexterity and navigation capabilities, the actuator should be able to bend in every direction. Consequently, a second model with two degrees of freedom in bending is presented (2-dof model). This actuator must be able to bend in every direction by selectively pressurizing one or two of the three pressurized channels. More channels would be redundant and the ratio between the cross-sectional area of the channels and the cross-sectional area of the actuator would be reduced.

It is important to take the limitations of the model into account for this optimization study, the bending being overestimated by the numerical model. At 0.14 bar, the 1-dof optimized model and the 2-dof optimized model achieve respectively a radius of curvature of 13.11 mm and 22.13 mm, where the numerical model of the implemented model bends with a radius of curvature of 34.93 mm. As expected, seeing the maximized surface, the 1-dof optimized model presents the best bending at the lower pressure. It is also interesting to observe that, based on this model, the 2-dof model present a higher bending that the model implemented in this work, despite a smaller pressure channel surface. This can be explained by the reduction in bending stiffness caused by the reduction of the soft body surface in the cross-section. Note that the simultaneous pressurization of two channels increases slightly the bending (of 5% at 0.14 bar). The value of 10 mm for the radius of curvature should theoretically be achieved at reasonable pressure values.

Fig. 6 Optimized designs. (a) One degree of freedom. (b) Two degrees of freedom.

3.4 Applications and use cases

Soft actuators for minimally invasive surgery navigation offer the potential to increase the patient safety and the surgeon dexterity while enabling to reach remote locations through natural orifices or small incisions [1, 3]. The actuator presented in this work could be used as an end effector for a soft steerable catheter, able to carry various MIS tools. A typical use case would be to use it as a visualization module. A camera can be placed at its tip, while the leads of the camera would be placed in the internal lumen channel, and act as strain limiting fibre. Its small size could allow reaching remote locations, and its bending capabilities could allow an increased field of vision and enhanced navigation capabilities, while its softness ensures the safety of the patient.

3.4.1 Bending stiffness of the MIS device

The bending capabilities of the actuator will be influenced by the bending stiffness of the leads of the MIS tool. To analyse this effect, the numerical model presented in subsection 2.3 has been adapted by implementing the leads as a cylinder (1.5 mm diameter), replacing the 0.6 mm diameter limiting fibre. The cylinder has been modelled as a linear elastic material, to study the influence of its Young's modulus on the bending of the actuator. The results are shown in Figure 7. The radius of curvature increases linearly with the bending stiffness, as expected. The logarithmic axes deform the linear approximation. The y-intercept of the linear approximation (18.69 mm) is close to the value neglecting the bending stiffness in the internal lumen, i.e. using a thread as limiting fibre (16.86 mm). The slight difference could be explained by the difference of deformation of the pressure channel, the MIS device limiting its expansion. This model allows to anticipate the maximal bending stiffness of a device, to reach a given angle at a given pressure, for a particular design. As an example, the bending stiffness of the device becomes non-negligible from around $1 \, \mathrm{Nmm}^2$ for this design. More generally, the high flexibility of soft actuators can be a drawback for some applications [7, 26]. This model allows to investigate further the overall bending stiffness of the structure depending on the carried MIS tool, and could be used to guide the design of the actuator for more specific applications.

3.4.2 Miniaturization

Miniaturizing the presented actuator is another challenge that could allow the steerable catheter to pass through the working channel of endoscopes, and reach even smaller locations of the human body. The effect of scaling down the actuator has been studied numerically on the non-optimized model. The same ratio of
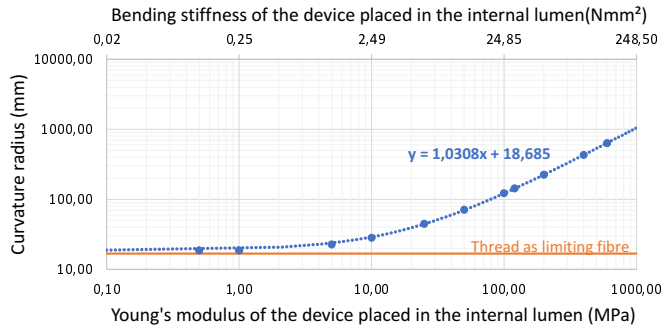
Fig. 7 Simulation results. Influence of the bending stiffness of the MIS device placed in the internal lumen of the actuator on the radius of curvature at 0.20 bar. The bending stiffness is given for the 1.5 mm diameter cylinder implemented.

surface between the pressure channel and the actuator is used for the miniaturization. The simulation results show no theoretical limitation to the miniaturization. Also, the miniaturized actuator requires less pressure to achieve the same radius of curvature. At 0.14 bar, the actuator model scaled down to an outer diameter of 2 mm achieves a radius of curvature of 15.29 mm, to be compared to the radius of curvature of 34.93 mm achieved by the the 5 mm model. This can be explained intuitively by the domination of the effect of the bending stiffness reduction, roughly proportional to the 4-th power of the outer diameter, while the pressure channel surface is roughly proportional to the square of the outer diameter. Those promising results must be put into perspective with technological and fragility limitations. The wall thickness is decreased to 0.24 mm for an outer diameter of 2 mm. The fabrication of such a geometry would be challenging with similar processes than those developed in this work, and the actuator would be more likely to break at lower pressures.

3.4.3 Future work direction

The results and the numerical model demonstrated the potential of the actuator. We believe that it could open new perspectives in terms of navigation, because of the small scale and bending capabilities of the presented actuator. However, challenges remain to integrate this end effector in a controllable steerable catheter, as the development of a control and navigation strategy, the study of its dynamic behaviour, and the integration of shape and contact sensors to provide feedback to the surgeon. The numerical model presented here allowed to develop a better understanding of the actuator, and could guide further design for more specific applications, and to develop adequate control strategies.

The risk of fluid leakage must be taken into consideration as well, as it would limit the potential of the actuator. As an example, the use of air to actuate the catheter forbids its use of intravascular procedures. Even if the risk is not negligible, a burst would not be dangerous for the patient, seeing the low pressure considered. To address these limitations, the possibility of replacing fluidic pressure by an expansive soft material should be investigated. Moreover, this alternative solution

could allow further miniaturization by avoiding the congestion of the pressure lines.

4 Conclusion

In this work, a proof of concept of a soft fluidic actuator for a steerable catheter has been designed, developed and characterized in terms of bending, radius of curvature, and blocking force. The 5 mm diameter prototype, having one degree of freedom in bending, is able to achieve a radius of curvature smaller than 10 mm and to develop forces above 40 mN for a pressure of 0.35 bar. A numerical model has been developed and compared to the experimental results. A finite element model has been developed and compared to the experimental results. Despite the highlighted limitations and an overestimation of the bending, the model properly captures the behaviour of the actuator. This model allowed to identify the key design parameters of the actuator, especially the ratio between the pressure channel surface and the actuator cross-section surface.

The miniaturization and the potential to carry devices with non-negligible bending stiffness have been studied using the numerical model. It showed no theoretical limit to miniaturization: at a given pressure, a scaled down actuator will achieve a smaller radius of curvature. Based on the results, optimized designs were proposed. The operating principle of an actuator able to bend in every direction has also been demonstrated.

Compliance with ethical standards

Conflict of Interest The authors declare that they have no conflict of interest.
Ethical approval This article does not contain any studies with human participants or animals performed by any of the authors.
Informed consent This article does not contain patient data.

References

1. Polygerinos P, Correll N, Morin SA, Mosadegh B, Onal CD, Petersen K, Cianchetti M, Tolley MT, Shepherd RF (2017) Soft robotics: Review of fluid-driven intrinsically soft devices; manufacturing, sensing, control, and applications in human-robot interaction. Advanced Engineering Materials 19(12):1700016, DOI 10.1002/adem.201700016, URL https://onlinelibrary.wiley.com/doi/abs/10.1002/adem.201700016, https://onlinelibrary.wiley.com/doi/pdf/10.1002/adem.201700016
2. Gorissen B, Reynaerts D, Konishi S, Yoshida K, Kim JW, De Volder M (2017) Elastic inflatable actuators for soft robotic applications. Advanced Materials 29(43):1604977, DOI 10.1002/adma.201604977, URL https://onlinelibrary.

wiley.com/doi/abs/10.1002/adma.201604977, https://onlinelibrary.wiley.com/doi/pdf/10.1002/adma.201604977

3. Cianchetti M, Laschi C, Menciassi A, Dario P (2018) Biomedical applications of soft robotics. Nature Reviews Materials 3(6):143–153, DOI 10.1038/s41578-018-0022-y, URL https://doi.org/10.1038/s41578-018-0022-y

4. Ali A, Plettenburg DH, Breedveld P (2016) Steerable catheters in cardiology: Classifying steerability and assessing future challenges. IEEE Transactions on Biomedical Engineering 63(4):679–693, DOI 10.1109/TBME.2016.2525785

5. Le HM, Do TN, Phee SJ (2016) A survey on actuators-driven surgical robots. Sensors and Actuators A: Physical 247:323–354, URL http://www.sciencedirect.com/science/article/pii/S0924424716302953

6. Burgner-Kahrs J, Rucker DC, Choset H (2015) Continuum robots for medical applications: A survey. IEEE Transactions on Robotics 31(6):1261–1280, DOI 10.1109/TRO.2015.2489500

7. Blanc L, Delchambre A, Lambert P (2017) Flexible medical devices: Review of controllable stiffness solutions. Actuators 6(3), DOI 10.3390/act6030023, URL https://www.mdpi.com/2076-0825/6/3/23

8. Hines L, Petersen K, Lum GZ, Sitti M (2017) Soft actuators for small-scale robotics. Advanced Materials 29(13):1603483, DOI 10.1002/adma.201603483, URL https://onlinelibrary.wiley.com/doi/abs/10.1002/adma.201603483, https://onlinelibrary.wiley.com/doi/pdf/10.1002/adma.201603483

9. De Greef A, Lambert P, Delchambre A (2009) Towards flexible medical instruments: Review of flexible fluidic actuators. Precision Engineering 33(4):311–321, URL http://www.sciencedirect.com/science/article/pii/S0141635908001190

10. Suzumori K (1989) Flexible microactuator. Trans Japan Soc Mech Eng Ser C 55(518):2547–2552

11. Wakimoto S, Suzumori K, Ogura K (2011) Miniature pneumatic curling rubber actuator generating bidirectional motion with one air-supply tube. Advanced Robotics 25(9-10):1311–1330, DOI 10.1163/016918611X574731, URL https://doi.org/10.1163/016918611X574731, https://doi.org/10.1163/016918611X574731

12. Inoue Y, Ikuta K (2016) Hydraulic driven active catheters with optical bending sensor. In: 2016 IEEE 29th International Conference on Micro Electro Mechanical Systems (MEMS), pp 383–386, DOI 10.1109/MEMSYS.2016.7421641

13. Gerboni G, Ranzani T, Diodato A, Ciuti G, Cianchetti M, Menciassi A (2015) Modular soft mechatronic manipulator for minimally invasive surgery (mis): overall architecture and development of a fully integrated soft module. Meccanica 50(11):2865–2878, DOI 10.1007/s11012-015-0267-0, URL https://doi.org/10.1007/s11012-015-0267-0

14. Elsayed Y, Vincensi A, Lekakou C, Geng T, Saaj CM, Ranzani T, Cianchetti M, Menciassi A (2014) Finite element analysis and design optimization of a pneumatically actuating silicone module for robotic surgery applications. Soft Robotics 1(4):255–262, DOI 10.1089/soro.2014.0016, URL https://doi.org/10.1089/soro.2014.0016, https://doi.org/10.1089/soro.2014.0016

15. Gorissen B, De Volder M, Reynaerts D (2018) Chip-on-tip endoscope incorporating a soft robotic pneumatic bending microactuator. Biomedical Microdevices 20(3):73, DOI 10.1007/s10544-018-0317-1, URL https://doi.org/10.1007/s10544-018-0317-1

16. Fraś J, Czarnowski J, Maciaś M, Główka J, Cianchetti M, Menciassi A (2015) New stiff-flop module construction idea for improved actuation and sensing. In: 2015 IEEE International Conference on Robotics and Automation (ICRA), pp 2901–2906, DOI 10.1109/ICRA.2015.7139595

17. Abidi H, Gerboni G, Brancadoro M, Fras J, Diodato A, Cianchetti M, Wurdemann H, Althoefer K, Menciassi A (2018) Highly dexterous 2-module soft robot for intra-organ navigation in minimally invasive surgery. The International Journal of Medical Robotics and Computer Assisted Surgery 14(1):e1875, DOI 10.1002/rcs.1875, URL `https://onlinelibrary.wiley.com/doi/abs/10.1002/rcs.1875`, e1875 RCS-17-0116.R2, `https://onlinelibrary.wiley.com/doi/pdf/10.1002/rcs.1875`

18. Sun Y, Song S, Liang X, Ren H (2016) A miniature soft robotic manipulator based on novel fabrication methods. IEEE Robotics and Automation Letters 1(2):617–623, DOI 10.1109/LRA.2016.2521889

19. Arezzo A, Mintz Y, Allaix ME, Arolfo S, Bonino M, Gerboni G, Brancadoro M, Cianchetti M, Menciassi A, Wurdemann H, Noh Y, Althoefer K, Fras J, Glowka J, Nawrat Z, Cassidy G, Walker R, Morino M (2017) Total mesorectal excision using a soft and flexible robotic arm: a feasibility study in cadaver models. Surgical Endoscopy 31(1):264–273, DOI 10.1007/s00464-016-4967-x, URL `https://doi.org/10.1007/s00464-016-4967-x`

20. Wang Z, Polygerinos P, Overvelde JTB, Galloway KC, Bertoldi K, Walsh CJ (2017) Interaction forces of soft fiber reinforced bending actuators. IEEE/ASME Transactions on Mechatronics 22(2):717–727, DOI 10.1109/TMECH.2016.2638468

21. Polygerinos P, Wang Z, Overvelde JTB, Galloway KC, Wood RJ, Bertoldi K, Walsh CJ (2015) Modeling of soft fiber-reinforced bending actuators. IEEE Transactions on Robotics 31(3):778–789, DOI 10.1109/TRO.2015.2428504

22. Yeoh OH (1993) Some forms of the strain energy function for rubber. Rubber Chemistry and Technology 66(5):754–771, DOI 10.5254/1.3538343, URL `https://doi.org/10.5254/1.3538343`, `https://doi.org/10.5254/1.3538343`

23. Kulkarni P (2015) Centrifugal forming and mechanical properties of silicone-based elastomers for soft robotic actuators. PhD thesis, New Brunswick

24. Steck D, Qu J, Kordmahale SB, Tscharnuter D, Muliana A, Kameoka J (2019) Mechanical responses of ecoflex silicone rubber: Compressible and incompressible behaviors. Journal of Applied Polymer Science 136(5):47025, DOI 10.1002/app.47025, URL `https://onlinelibrary.wiley.com/doi/abs/10.1002/app.47025`, `https://onlinelibrary.wiley.com/doi/pdf/10.1002/app.47025`

25. Garriga-Casanovas A, Collison I, Rodriguez y Baena F (2018) Toward a common framework for the design of soft robotic manipulators with fluidic actuation. Soft Robotics 5(5):622–649, DOI 10.1089/soro.2017.0105, URL `https://doi.org/10.1089/soro.2017.0105`, pMID: 30161015, `https://doi.org/10.1089/soro.2017.0105`

26. Shiva A, Stilli A, Noh Y, Faragasso A, Falco ID, Gerboni G, Cianchetti M, Menciassi A, Althoefer K, Wurdemann HA (2016) Tendon-based stiffening for a pneumatically actuated soft manipulator. IEEE Robotics and Automation Letters 1(2):632–637, DOI 10.1109/LRA.2016.2523120